HHS Public Access

Author manuscript

Angew Chem Int Ed Engl. Author manuscript; available in PMC 2024 September 25.

Published in final edited form as:

Angew Chem Int Ed Engl. 2023 September 25; 62(39): e202309258. doi:10.1002/anie.202309258.

Modular Functionalization of Metal-Organic Frameworks for Nitrogen Recovery from Fresh Urine

Lei Guo[a,b,c], **Yi Zhang**[b], **Silvio Osella**[d,e], **Samuel M. Webb**[f], **Xue-jing Yang**[a], **William A. Goddard III**[e], **Michael R. Hoffmann**[b]

[a]National Engineering Laboratory for Industrial Wastewater Treatment and State Key Laboratory of Chemical Engineering, East China University of Science and Technology, Shanghai 200237, China

[b]Linde Laboratories, California Institute of Technology, Pasadena, California 91125, United States

[c]Present address: Department of Civil Engineering, University of Arkansas, Fayetteville, Fayetteville, Arkansas 72701, United States

[d]Chemical and Biological Systems Simulation Lab, Center of New Technologies, University of Warsaw, Banacha 2C, 02-097 Warsaw, Poland

[e]Materials and Process Simulation Center, California Institute of Technology, Pasadena, CA 91125, United States

[f]Stanford Synchrotron Radiation Lightsource, SLAC National Accelerator Laboratory, 2575 Sand Hill Rd., Menlo Park, CA 94025, United States

Abstract

Nitrogen recovery from wastewater represents a sustainable route to recycle reactive nitrogen (Nr). It can reduce the demand of producing Nr from the energy-extensive Haber-Bosch process and lower the risk of causing eutrophication simultaneously. In this aspect, source-separated fresh urine is an ideal source for nitrogen recovery given its ubiquity and high nitrogen contents. However, current techniques for nitrogen recovery from fresh urine require high energy input and are of low efficiencies because the recovery target, urea, is a challenge to separate. In this work, we developed a novel fresh urine nitrogen recovery treatment process based on modular functionalized metal-organic frameworks (MOFs). Specifically, we employed three distinct modification methods to MOF-808 and developed robust functional materials for urea hydrolysis, ammonium adsorption, and ammonia monitoring. By integrating these functional materials into our newly developed nitrogen recovery treatment process, we achieved an average of 75% total nitrogen reduction and 45% nitrogen recovery with a 30-minute treatment of synthetic fresh urine. The nitrogen recovery process developed in this work can serve as a sustainable and efficient nutrient management that is suitable for decentralized wastewater treatment. This work also

leiguo@uark.edu, xj.yang@ecust.edu.cn, wag@caltech.edu.
[+]These authors contributed equally.

Conflict of Interest: The authors declare no conflict of interest.

Supporting Information

The authors have cited additional references within the Supporting Information.[64–74]

provides a new perspective of implementing versatile advanced materials for water and wastewater treatment.

Social media promotion:

Modular Functionalization of **#Metal-Organic Frameworks** for Nitrogen Recovery from Fresh Urine (Hoffmann and coworkers) @LeiGuo20 @UArkansas @CaltechCCE

Graphical Abstract

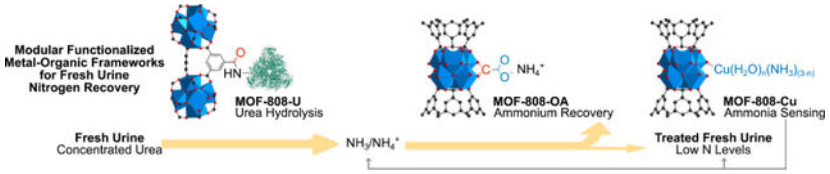

Modular functionalized MOF-808 derivatives were deliberately designed and integrated in a newly developed nitrogen recovery treatment process targeting fresh urine. Three distinct modification methods were applied for the development of functional MOFs which deliver efficient nitrogen conversion, recovery, detection, and all contributing to high fresh urine nitrogen recovery that is suitable for decentralized wastewater treatment.

Keywords

Metal-Organic Frameworks; Nitrogen Recovery; Urine; Renewable Resources; Waste Prevention

Introduction

The nitrogen cycle is essential to the ecosystem.[1] The bioavailability of reactive nitrogen (Nr) directly impacts the ecosystem processes and is closely related to and influenced by anthropogenic activities. Among all Nr species, ammonia and urea are essential agricultural and industrial chemicals that are tightly coupled with human activities. While the highly energy-extensive Haber-Bosch process converts atmospheric nitrogen into Nr to promote food production and economic growth, inadequate downstream management of Nr in wastewater can in turn harm the ecosystem, such as eutrophication. Human urine, which is probably the most ubiquitous nitrogen source that contains high density of urea, is a major contributor to Nr discharge in municipal wastewater.[2] Since the majority of the world population does not have access to nutrient-eliminating wastewater treatment plants,[3] recovery of nitrogen from urine, especially at source (e.g., urine source separation systems), can greatly simplify municipal wastewater treatment processes, preventing eutrophication while simultaneously recycling Nr for agricultural and industrial applications. Overall, nitrogen recovery from urine could be a central step to promote the practice of the water-food-energy nexus.

Nitrogen from urine is captured either in the form of ammonia/ammonium in stored urine or urea in fresh urine (Scheme 1a). Urea is difficult to separate from fresh urine because it is neutral and possesses high water solubility and affinity. Current urea recovery processes

mainly rely on volume reduction,[4,5] membrane treatment,[6,7] and precipitation,[8] all of which require extensive external input of energy or chemicals. By contrast, ammonia/ammonium are more technically feasible recovery targets, because ammonia is volatile, and ammonium can be readily separated based on electrostatic interactions. Common ammonia/ammonium recovery methods include ion exchange,[9–12] stripping,[13–16] electrochemical treatment,[14,17–19] and precipitation.[13,20–22] However, ammonia/ammonium recovery from stored urine relies heavily on the complete hydrolysis of urea which can take up to days depending on the specific environment.[21,23,24] This duration further requires ample space for urine storage, efforts for urine collection and transportation, and sophisticated urine stabilization prior to the nitrogen recovery treatment[25]— all of which lead to higher capital costs and maintenance expenses.[26,27] Additionally, a substantial amount of ammonia-nitrogen is lost during the long-term urine storage period,[26] which fundamentally reduces the overall nitrogen recovery efficiency of the treatment process.

To tackle the challenges in the current urine nitrogen recovery techniques, we herein report our work on developing an array of modular functionalized metal-organic frameworks (MOFs) that are deliberately designed for a novel fresh urine nitrogen recovery treatment process. We selected a highly water stable and porous zirconium metal-organic framework, MOF-808, as the pristine material, which has been reported to have high thermal and water stability, porosity, and tunability of physicochemical properties. MOF-808 has been studied extensively for a variety of water treatment applications, including sensing, desalination, and pollutant removal by adsorption or catalytic oxidation and reduction.[28–33] We present herein the first example of employing MOF-808 in toilet wastewater treatment (Scheme 1) for nutrient management. Specifically, we first synthesized urease-incorporated composite, MOF-808-U, for rapid urea hydrolysis to convert urea to ammonia in a timely manner. We further designed oxalate-decorated MOF-808-OA for efficient ammonium capture and recovery. Finally, Cu(II)-modified MOF-808, MOF-808-Cu, was applied for real-time ammonia monitoring. All functionalized MOFs have been well characterized with systematic experimental and computational studies. We further assembled all three functionalized MOFs into a treatment train. With the urea hydrolysis process significantly accelerated and the hydrolysis product readily captured *in situ*, we were able to achieve rapid and efficient nitrogen recovery in fresh urine with no extensive urine storage required (Scheme 1b). Furthermore, on-site ammonia-nitrogen monitoring can provide real-time nitrogen concentrations in the treated effluent as quality control of operation of each treatment step. As no substantial urine storage is required, this newly developed compact treatment process is more applicable for decentralized toilet wastewater treatment in rural and developing communities.

Results and Discussion

Urea hydrolysis is ubiquitous in nature and is naturally catalyzed by urease generated by microbes in a slow and uncontrollable manner.[34] As a result, different studies have reported quite variable rates of ureolysis, indicating a high dependence on the local environment. For example, Udert *et al.* reported that 960 g urea-N d^{-1} could be hydrolyzed in NoMix pipes and 180 g urea-N d^{-1} in collection tanks.[34] A study by Liu *et al.* indicated complete urea hydrolysis could take up to 2 to over 6.5 days.[23] A more recent study focusing on urine

collection on a building-scale by Jagtap *et al.* demonstrated that complete urea hydrolysis could be achieved in 8 h.[24] This variable nature of urea hydrolysis inevitably results in unpredictable processing time and efficiency from batch to batch, creating uncertainty in a centralized facility. Consequently, it is necessary to incorporate long-term and large-scale urine storage units in onsite urine treatment for complete urea conversion prior to nitrogen recovery, which increases capital costs and makes it challenging for decentralized treatment systems (e.g., single family household).

In order to significantly boost urea hydrolysis kinetics in fresh urine to compensate for the natural processes, we developed an artificial urease-enriched environment with MOF-808. Jackbean urease was immobilized onto MOF-808 backbone via strong covalent bonds, providing a MOF-urease composite that can serve as a highly efficient, stable, and more sustainable catalyst for urine hydrolysis. Optimizing the previously reported procedure and incorporating N-hydroxysuccinimide to increase the stability of the intermediate ester in aqueous solutions,[35,36] we successfully grafted urease onto the MOF-808 backbone by forming amide bonds between the amino residues on urease and the terminal carboxylate groups on MOF-808 (Scheme 2). This MOF-urease composite is designated as MOF-808-U, for which we determined the loading capacity to be 1.7 g urease/g MOF-808. Successful immobilization of urease was confirmed by FT-IR spectra, where both the amide I (1714 cm^{-1}) and amide II bands (1654 cm^{-1}) from free urease were observed in the spectrum of MOF-808-U (Figure S1).[37] The crystalline structure of the MOF was well-maintained during the modification process as confirmed by powder X-ray diffraction (PXRD) measurements (Figure 1a), and the morphology of the crystallites remained unaltered as evidenced by SEM images (Figure S8 and S9), demonstrating that MOF-808 provides a robust backbone for materials engineering purposes.

We first assayed the catalytic activity of the immobilized urease and plotted the Michaelis–Menten curves for both MOF-808-U and free urease in Figure 1b. We found that MOF-808-U possesses a Michaelis–Menten constant ($K_{m\ (MOF\text{-}808\text{-}U)}$ = 25.15 mM) very similar to that of free urease ($K_{m\ (free\ urease)}$ = 24.80 mM), indicating that the affinity of MOF-808-U towards urea is almost identical to that of the free enzyme. We observed a decrease of k_{cat} for MOF-808-U (Table S1), which is commonly found in enzyme immobilization processes.[38–41] Most importantly, stability of the immobilized urease was significantly enhanced in MOF-808-U (Figure 1c). While free urease almost completely denatured after being stored in an aqueous solution for one day, MOF-808-U still possessed almost 40% of its original activity after one day, and maintained around 20% activity after six days. This unprecedented prolonged stability of MOF-808-U likely originates from the multipoint strong covalent attachment of urease onto the MOF backbone that maintains the intrinsic structural integrity of the enzyme.[42,43] Taken together, our results for MOF-808-U demonstrate its prolonged and kinetic-efficient performance in converting urea.

Now that urea in fresh urine is converted to ammonium, a more feasible product for capture, with MOF-808-U, our next step is to design an efficient adsorbent to recover as-produced hydrolysis product. One major driving force for ammonium capture in common adsorbents is electrostatic interaction, exemplified by negatively charged functionalization of the adsorbents.[9,44] In order to introduce ammonium binding affinity to MOF-808 backbone,

we selected a series of dicarboxylate compounds, namely oxalic acid (OA), malonic acid (MA), and succinic acid (SA), as anionic functional group. For each dicarboxylate compound, one carboxylate stitches strongly to the Zr_6O_8 cluster via bidentate chelating,[45] whereas the other remains dangling inside the pore to serve as the ammonium adsorption sites (Scheme 3). Successful incorporation of MA and SA was confirmed and quantified with ^{1}H NMR spectra of the digested samples (Figure S6 and S7), whereas the incorporated OA was determined via colorimetric assay of the digested MOF-808-OA.[46] FT-IR spectra further confirmed the successful introduction of the dicarboxylic acids (Figure S2). The absorbance corresponding to the carbonyl stretching from formate in pristine MOF-808 shifted from 1704 cm^{-1} to 1697 cm^{-1}, 1699 cm^{-1}, and 1703 cm^{-1} in MOF-808-OA, MOF-808-MA, and MOF-808-SA, respectively, which follows the trend in molecular compounds.[47] At the same time, the MOF-808 backbone remained intact with its high crystallinity confirmed by the almost identical PXRD pattern (Figure 2a) and morphology (Figure S10–12) to that of pristine MOF-808. These results again corroborate MOF-808 as a robust and versatile material for various functionalization.

With the materials in hand, we examined ammonium uptake performance of four MOF-808-based adsorbents. The ammonium adsorption isotherms were fitted best with the Langmuir-Freundlich model for all materials (Figure 2b), with the capture capacity as well as other adsorption isotherm parameters listed in Table S2. While all adsorbents exhibited a decent level of ammonium capture, MOF-808-OA exhibited the highest ammonium capture capacity (Q_e = 113 mg g^{-1}), followed by MOF-808-MA, MOF-808-SA, and pristine MOF-808. Notably, MOF-808-OA is among the most efficient ammonium adsorbents based on its high capture capacity.[44] Time-course adsorption measurements were further carried out. Ammonium capture by all materials was kinetically efficient (Figure 2c), and MOF-808-OA again outperformed the others, reaching adsorption equilibrium within 1 min.

The favorable properties of MOF-808-OA over the other functional MOF-808 derivatives indicate that MOF functionalization plays a major role in their ammonium binding affinity. To better understand how the above pore engineering influenced the ammonium uptake behavior, we carried out molecular dynamics (MD) simulations on all four MOF materials (see Section 8 of the SI for more details). After 20 ns of MD (using the NVT ensemble) for each system, in which the ammonium ions were added according to the experimental concentrations, we observed strong interactions between the carboxyl oxygen atoms of the different acids (OA, MA and SA) with the ammonium nitrogen atoms, which was analyzed by the radial distribution function (RDF) (Figure 2d). This analysis leads to an average distance of 0.285 nm between ammonium nitrogens and carboxylic oxygens, indicating the formation of a close-contact ionic complex in which no water is involved.Integrating the RDF leads to 1.24, 3.33 and 2.74 oxygen atoms per ammonium nitrogen for MOF-808-OA, MOF-808-MA, and MOF-808-SA, respectively (Figure S18 and Table S4), which shows the synergetic effect of both binding affinities between carboxylates and ammonium and the amount of available binding sites within the pores. The decreasing pore sizes due to the incorporation of functionality moieties (Table S5) further allows ammonium ions to get closer to more oxygen atoms. In comparison, the pristine MOF-808 presented a much longer average distance of 0.445 nm between the ammonium nitrogen and the formate hydrogen, corresponding to having two hydrogen atoms close to the ammonium ions. This suggests

that a layer of water is present between the ions, weakening the MOF backbone-ammonium interaction.

To further quantify the strength of these ammonium-MOF backbone interactions, we carried out the two-phase thermodynamic (2PT) analysis [48–50] to compute the adsorption free energy differences between the ammonium in water compared to the cases when they were adsorbed in the MOF. Our calculations indicate that MOF-808-OA presents the strongest adsorption free energy (−4537 kcal/mol), followed by MOF-808-MA (−4303 kcal/mol) and MOF-808-SA (−3109 kcal/mol) (Figure S23). These computational results demonstrate the same trend found in our experimental adsorption data. In comparison, the pristine MOF-808 showed an adsorption free energy of only −2172 kcal/mol, confirming the added benefit of the incorporation of carboxylates in the MOF structure for ammonium adsorption. These MD calculations also supported the experimental findings that the best candidate is MOF-808-OA, which we then used as the ammonium adsorbent for the remainder of our study.The regeneration of MOF-808-OA, an important property for sustainability in nitrogen recovery, was evaluated further. We used sodium nitrate solution to treat ammonium-saturated MOF-808-OA, during which sodium ions were exchanged with ammonium to regenerate MOF-808-OA carrying sodium ions, providing ammonium nitrate in solution as the nitrogen recovery product. MOF-808-OA could be reused for at least 10 cycles while retaining the original excellent ammonium capture capacity (Figure 2e), and we were able to achieve near complete recovery of ammonium (Figure 2f). These results demonstrate MOF-808-OA to be a durable adsorbent for nitrogen recovery in water treatment.

Besides onsite nitrogen coversion and recovery as discussed above, online monitoring of ammonia levels in pre- and post-treated water is essential to the water management process to ensure that desired treatment is carried out successfully. The commonly used Berthelot method requires several reaction steps and reagents (e.g., basic conditions, hypochlorite, and phenol) followed by UV determination of the concentration,[51,52] which complicates their on-site implementation. Ammonia electrodes, on the other hand, are generally limited by the longevity of the selective membranes. The emergence of innovative nanomaterials has opened up new avenues for ammonia sensing.[53,54] While most current sensing systems afford nanomolar detection limits and a working range up to millimolar, they are not suitable for the direct use in toilet wastewater treatment because of the ultrahigh ammonia levels in urine. Therefore, a sensitive, accurate, and feasible on-site ammonia sensor with a working window covering high ammonia concentrations is highly desired in nitrogen recovery in toilet wastewater. Towards this end, we developed another MOF-808-based functional material to serve as the online ammonia indicator.

Inspired by the well-known molecular Cu(II)-ammonia complex that possesses a distinguishing dark blue color, we selected Cu(II) to be incorporated onto the MOF-808 backbone intended for colorimetric sensing of ammonia, with the product designated as MOF-808-Cu. MOF-808-Cu was readily synthesized by impregnating MOF-808 with a $CuSO_4$ methanolic solution (Scheme 4), where the powder color changed from white to pale green upon the Cu incorporation. The highly crystalline structure of MOF-808 was again well-maintained upon the modification (Figure 3a). In order to determine the Cu coordination environment, we performed extended X-ray absorption fine structure (EXAFS)

analysis on MOF-808-Cu. Figure 3b shows the data and the results of the best fit in the amplitude and real portions of the Fourier Transform. The full fitting information is provided in Table S6 in the Supplementary Information. The data and fitting results are consistent with similar previous works[55] that show Cu is coordinated by four oxygen atoms at the distance of 1.92 Å and is connected to the MOF framework with a distance of 3.19 Å to Zr atoms. The Zr neighbor in the EXAFS is of low amplitude, with a relatively large Debye-Waller disorder parameter indicative of Cu's monodentate binding mode to Zr (Scheme 4). SEM-EDS mapping further indicated that Cu was homogeneously distributed throughout the MOF backbone (Figure 3c and Figure S13), and Zr to Cu atomic ratio was quantified to be 2.18:1 by inductively coupled plasma mass spectrometry (ICP-MS). Additionally, strong absorbance within the 1200–900 cm^{-1} region in the FT-IR spectrum of MOF-808-Cu is assigned to the vibration of Zr-O-Cu bonds as well as sulfate (Figure S3).[56–58]

We then evaluated MOF-808-Cu's response to ammonia. Upon exposure to ammonia solutions, the solids immediately changed color from pale green to blue, a phenomenon similar to that observed for a molecular copper-ammonia complex. This ammonia-induced Cu's coordination environment change was further evidenced with XAS analysis. X-ray spectroscopy was collected with an aliquot of NH_3 solution added to MOF-808-Cu immediately before measurement. The EXAFS showed that the Cu remains coordinated to the MOF backbone via the second shell of Zr, but the Cu near edge data (Figure 3d) shows a change in the edge profile that is consistent with binding of Cu to NH_3 ligands.[59] This colorimetric response was also observed with UV−Vis diffuse reflectance spectra (Figure S18) which showed a significant blue shift of the UV-Vis absorbance maximum from 757 nm to 667 nm. Furthermore, the obvious color change could be readily quantified using a digital camera (e.g., a smartphone camera) (insert of Figure 3e). By extracting readouts from red (R), green (G), and blue (B) channels from the image of Figure 3e, a linear curve within the range of 200–4000 ppm ammonia nitrogen could be constructed from the data points obtained from the R and G channels, where R channels afforded the highest linearity (Figure 3e and Figure S26–28). Notably, MOF-808-Cu can also be reused for at least 5 cycles with mild heat treatment to regenerate Cu (II) coordination sites while readings of the R channel remained mostly constant (within < 5% of fluctuation) (Figure 3f). Taken together, we have demonstrated the feasibility of using MOF-808 for task-oriented design and modification, and we have presented MOF-808-Cu's potential of serving as a real-time on-site ammonia-nitrogen sensor suitable for urine treatment systems.

Upon the successful synthesis, characterization, and evaluation of all three functionalized MOF materials, we included them all together and developed a prototype system targeting nitrogen recovery from fresh urine (Figure 4a). The working prototype encompasses two major counterparts that can work independently: (1) 30 min of nitrogen conversion and (2) 30 min of nitrogen removal and recovery. First, fresh urine was incubated with MOF-808-U for 30 min to hydrolyze the majority, if not all, of the urea. Hydrolyzed effluent was then mixed with MOF-808-OA for 15 min to ensure that the adsorption of ammonium reached equilibrium given the fast kinetics of the ammonium adsorption (Figure 2d). Saturated MOF-808-OA was then regenerated with $NaNO_3$ with a 15 min mixing, yielding ammonium exchanged with sodium in the regeneration solution and the adsorption sites free and ready for the next run. During nitrogen capture and recovery, MOF-808-U could accommodate

additional incoming fresh urine in the next cycle to ensure a continuous operation of the treatment train. Therefore, the current setup allows for the treatment of fresh urine every 30 min when functioning consecutively.

As a proof of concept, we performed five cycles of treatment with synthetic fresh urine (prepared following a previously reported recipe).[60] Given the high concentration of nitrogen in the initial influent ([Urea-N] = 7000 ppm), high loads of MOF-808-U and MOF-808-OA (200 g/L) was required for sufficient nitrogen removal. Concentrations of urea and ammonium were measured after each treatment to determine the overall nitrogen removal and recovery efficiency. As shown in Figure 4b, the first three cycles of the treatment resulted in ~80% total nitrogen removal, which meets the ISO30500 standard for 70% total nitrogen reduction.[61] A slight drop of total nitrogen reduction efficiency was observed in the fourth and the fifth cycle, but the majority of nitrogen (67% and 62%) could still be removed with a 30 min treatment. Total nitrogen recovery efficiency, however, followed the opposite trend — relatively low for the first two cycles and increased to 48%−64% for the later three cycles. This phenomenon was due to the near-complete urea hydrolysis during the first three cycles (Figure 4b), which resulted in high ammonium ion formation coupled with evaporative loss of ammonia leading to reduced adsorption of ammonium.[62] During the subsequent two cycles where the kinetics of urea hydrolysis synchronized with the kinetics of ammonium uptake, the loss of ammonia was significantly reduced as the hydrolysis product was readily captured by MOF-808-OA, resulting in a total recovery efficiency reaching to the total removal efficiency. Overall, the current treatment process yielded an average of 75% total nitrogen reduction and an average of 45% nitrogen recovery in five cycles. Furthermore, MOF-808-Cu, the *in situ* chromophoric probe, gave the anticipated color changes that could be visually observed (Figure 4c). While the blue color (top) indicated that significant ammonium was generated by MOF-808-U, the change of color to green (bottom) demonstrated substantial removal of ammonium by MOF-808-OA. Such color changes could be observed for all five cycles, indicating that urea hydrolysis, ammonium capture, and regeneration of MOF-808-OA were carried out successfully for each cycle. Based on the above results, it is clear that all three MOF materials functioned in the developed treatment process as designed and indeed afforded rapid and high nitrogen recovery from fresh urine.

Conclusion

In summary, we developed a nutrient treatment process that, for the first time, to our knowledge, achieved simultaneous nitrogen conversion, removal, recovery, and monitoring from fresh urine. Efficient nitrogen reduction was achieved in the effluent, which significantly reduced the burden for downstream treatment (e.g., biological and electrochemical treatment in onsite systems) to remove nutrients and minimize the risk of eutrophication. The entire treatment process can be operated successively every 30 min, which circumvents the requirement for wastewater collection and transportation and renders this treatment process much more suitable for decentralized toilet wastewater treatment. Nitrogen recovery further provides valuable nitrogen-rich byproducts (NH_4NO_3) as potential fertilizers for agricultural applications. With more ongoing works on optimizing the treatment efficiency, materials longevity, and cost consumption, the current treatment

process is still competitive to alternate nitrogen recovery techniques (a detailed cost analysis discussion is provided in the Supporting Information). Integrating both nitrogen conversion and recovery, our treatment process provides a more compact, customized, and resilient nutrient management compared to centralized treatment. Taken together, the fresh urine treatment system developed in this work has the potential to transform into novel decentralized urine treatment processes, contribute to the water-food-energy nexus, and especially benefit rural and developing communities.

The MOF materials used in this study showcase their ultrahigh versatility and modularity to be functionalized towards specific environmental applications with deliberate design. With more works reporting large-scale synthesis of high quality MOFs,[63] this class of materials hold high promise for future implementation in environmental applications. This work renders itself as the first example of employing MOFs for toilet wastewater treatment and fulfilling multiple tasks. Together with other reports of MOFs used for removal or sensing of target pollutants in water, we anticipate that MOFs possess great potential as robust and versatile innovative materials for efficient and sustainable water and wastewater management.

Supplementary Material

Refer to Web version on PubMed Central for supplementary material.

Acknowledgements

X.J.Y. acknowledges the National Key Projects for Fundamental Research and Development of China (Grant No. 2019YFC1906700), the National Natural Science Foundation for Outstanding Young Scholars (Grant No. 22222602), the National Natural Science Foundation of China (Grant No. 21876049), and Shanghai Technology Innovation Program of Technical Center (20DZ2250600). S.O. acknowledges the Polish National Science Center (grant no. UMO-2020–39-I-ST4–01446) and the Polish National Agency for Academic Exchange under the Bekker program (grant no. PPN/BEK/2020/1/00053/U/00001). W.A.G. was supported by the NIH (R01HL155532). Use of the Stanford Synchrotron Radiation Lightsource, SLAC National Accelerator Laboratory, is supported by the U.S. Department of Energy, Office of Science, Office of Basic Energy Sciences under Contract No. DE-AC02–76SF00515. The SSRL Structural Molecular Biology Program is supported by the DOE Office of Biological and Environmental Research, and by the National Institutes of Health, National Institute of General Medical Sciences (P30GM133894). The contents of this publication are solely the responsibility of the authors and do not necessarily represent the official views of NIGMS or NIH. L.G acknowledges helpful discussion with Dr. Shang Jia.

References

[1]. Whalen JM, Matlin SA, Holme TA, Stewart JJ, Mahaffy PG, ACS Sustain. Chem. Eng. 2022, 10, 12933–12947.

[2]. Jimenez J, Bott C, Love N, Bratby J, Water Environ. Res. 2015, 87, 2120–2129. [PubMed: 26652123]

[3]. Larsen TA, Water Sci. Technol. 2011, 63, 2535–2541. [PubMed: 22049745]

[4]. Senecal J, Vinnerås B, Sci. Total Environ. 2017, 586, 650–657. [PubMed: 28215808]

[5]. Marepula H, Courtney CE, Randall DG, Chem. Eng. J. Adv. 2021, 8, 100174.

[6]. Ray H, Perreault F, Boyer TH, Environ. Sci. Water Res. Technol. 2019, 5, 1993–2003.

[7]. Xu L, Ding R, Mao Y, Peng S, Li Z, Zong Y, Wu D, Water Res. 2021, 202, 117423. [PubMed: 34284122]

[8]. Behrendt J, Arevalo E, Gulyas H, Niederste-Hollenberg J, Niemlec A, Zhou J, Otterpohl R, Water Sci. Technol. J. Int. Assoc. Water Pollut. Res. 2002, 46, 341–346.

[9]. Huang J, Kankanamge NR, Chow C, Welsh DT, Li T, Teasdale PR, J. Environ. Sci. 2018, 63, 174–197.

[10]. Clark B, Tarpeh WA, Chem. – Eur. J. 2020, 26, 10099–10112. [PubMed: 32500617]

[11]. Tarpeh WA, Udert KM, Nelson KL, Environ. Sci. Technol. 2017, 51, 2373–2381. [PubMed: 28098981]

[12]. Manto MJ, Xie P, Keller MA, Liano WE, Pu T, Wang C, Chemosphere 2018, 198, 501–509. [PubMed: 29427951]

[13]. Xu K, Zhang C, Li J, Cheng X, Wang C, Water Sci. Technol. 2016, 75, 155–164.

[14]. Christiaens MER, Gildemyn S, Matassa S, Ysebaert T, De Vrieze J, Rabaey K, Environ. Sci. Technol. 2017, 51, 13143–13150. [PubMed: 29112388]

[15]. Jagtap N, Boyer TH, Environ. Sci. Water Res. Technol. 2018, 4, 1639–1650.

[16]. Christiaens MER, Udert KM, Arends JBA, Huysman S, Vanhaecke L, McAdam E, Rabaey K, Water Res. 2019, 150, 349–357. [PubMed: 30530129]

[17]. Kuntke P, Śmiech KM, Bruning H, Zeeman G, Saakes M, Sleutels THJA, Hamelers HVM, Buisman CJN, Water Res. 2012, 46, 2627–2636. [PubMed: 22406284]

[18]. Kuntke P, Rodrigues M, Sleutels T, Saakes M, Hamelers HVM, Buisman CJN, ACS Sustain. Chem. Eng. 2018, 6, 7638–7644. [PubMed: 29888142]

[19]. Tarpeh WA, Barazesh JM, Cath TY, Nelson KL, Environ. Sci. Technol. 2018, 52, 1453–1460. [PubMed: 29303251]

[20]. Wei SP, van Rossum F, van de Pol GJ, Winkler M-KH, Chemosphere 2018, 212, 1030–1037. [PubMed: 30286532]

[21]. Kabdaşlı I, Tünay O, İşlek Ç, Erdinç E, Hüskalar S, Tatlı MB, Water Sci. Technol. 2006, 53, 305–312. [PubMed: 16889267]

[22]. Tan X, Yu R, Yang G, Wei F, Long L, Shen F, Wu J, Zhang Y, Environ. Sci. Pollut. Res. 2021, 28, 5625–5636.

[23]. Liu Z, Zhao Q, Wang K, Lee D, Qiu W, Wang J, J. Environ. Sci. 2008, 20, 1018–1024.

[24]. Jagtap NS, Boyer TH, J. Environ. Chem. Eng. 2020, 8, 103964.

[25]. Yang W, Li J, Yang X, Front. Sustain. 2021, 2, 710739.

[26]. Larsen TA, Riechmann ME, Udert KM, Water Res. X 2021, 100114. [PubMed: 34693239]

[27]. Maurer M, Pronk W, Larsen TA, Water Res. 2006, 40, 3151–3166. [PubMed: 16949123]

[28]. Furukawa H, Gándara F, Zhang Y-B, Jiang J, Queen WL, Hudson MR, Yaghi OM, J. Am. Chem. Soc. 2014, 136, 4369–4381. [PubMed: 24588307]

[29]. Li Z-Q, Yang J-C, Sui K-W, Yin N, Mater. Lett. 2015, 160, 412–414.

[30]. Zheng H-Q, Liu C-Y, Zeng X-Y, Chen J, Lü J, Lin R-G, Cao R, Lin Z-J, Su J-W, Inorg. Chem. 2018, 57, 9096–9104. [PubMed: 29993241]

[31]. Chen X, Chen D, Li N, Xu Q, Li H, He J, Lu J, ACS Appl. Mater. Interfaces 2020, 12, 39227–39235. [PubMed: 32805808]

[32]. Ji C, Yu H, Lu J, Ren Y, Lv L, Zhang W, ACS Appl. Mater. Interfaces 2021, 13, 23833–23842. [PubMed: 33973777]

[33]. Plonka AM, Grissom TG, Musaev DG, Balboa A, Gordon WO, Collins-Wildman DL, Ghose SK, Tian Y, Ebrahim AM, Mitchell MB, Hill CL, Morris JR, Frenkel AI, Chem. Mater. 2019, 31, 9904–9914.

[34]. Udert KM, Larsen TA, Biebow M, Gujer W, Water Res. 2003, 37, 2571–2582. [PubMed: 12753834]

[35]. Guo L, Jia S, Diercks CS, Yang X, Alshmimri SA, Yaghi OM, Angew. Chem. Int. Ed. 2020, 59, 2023–2027.

[36]. Mattson G, Conklin E, Desai S, Nielander G, Savage MD, Morgensen S, Mol. Biol. Rep. 1993, 17, 167–183. [PubMed: 8326953]

[37]. Liang W, Xu H, Carraro F, Maddigan NK, Li Q, Bell SG, Huang DM, Tarzia A, Solomon MB, Amenitsch H, Vaccari L, Sumby CJ, Falcaro P, Doonan CJ, J. Am. Chem. Soc. 2019, 141, 2348–2355. [PubMed: 30636404]

[38]. Rodrigues RC, Ortiz C, Berenguer-Murcia Á, Torres R, Fernández-Lafuente R, Chem. Soc. Rev. 2013, 42, 6290–6307. [PubMed: 23059445]

[39]. Liese A, Hilterhaus L, Chem. Soc. Rev. 2013, 42, 6236–6249. [PubMed: 23446771]

[40]. Bolivar JM, Nidetzky B, Biochim. Biophys. Acta BBA - Proteins Proteomics 2020, 1868, 140333. [PubMed: 31778816]

[41]. Liang W, Wied P, Carraro F, Sumby CJ, Nidetzky B, Tsung C-K, Falcaro P, Doonan CJ, Chem. Rev. 2021, 121, 1077–1129. [PubMed: 33439632]

[42]. Garcia-Galan C, Berenguer-Murcia Á, Fernandez-Lafuente R, Rodrigues RC, Adv. Synth. Catal. 2011, 353, 2885–2904.

[43]. Mateo C, Palomo JM, Fernandez-Lorente G, Guisan JM, Fernandez-Lafuente R, Enzyme Microb. Technol. 2007, 40, 1451–1463.

[44]. Han B, Butterly C, Zhang W, He J, Chen D, J. Clean. Prod. 2021, 283, 124611.

[45]. Lyu H, Chen OI-F, Hanikel N, Hossain MI, Flaig RW, Pei X, Amin A, Doherty MD, Impastato RK, Glover TG, Moore DR, Yaghi OM, J. Am. Chem. Soc. 2022, 144, 2387–2396. [PubMed: 35080872]

[46]. Bergerman J, Elliot JS, Anal. Chem. 1955, 27, 1014–1015.

[47]. Craver CD, Desk Book of Infrared Spectra, The Coblentz Society, 1982.

[48]. Lin S-T, Blanco M, Goddard WA, J. Chem. Phys. 2003, 119, 11792–11805.

[49]. Lin S-T, Maiti PK, Goddard WA, J. Phys. Chem. B 2010, 114, 8191–8198. [PubMed: 20504009]

[50]. Pascal TA, Lin S-T, Iii WAG, Phys. Chem. Chem. Phys. 2010, 13, 169–181. [PubMed: 21103600]

[51]. Weatherburn MW, Anal. Chem. 1967, 39, 971–974.

[52]. EPA Method 350.1: Determination of Ammonia Nitrogen by Semi-Automated Colorimetry, 2019.

[53]. Mahmud MAP, Ejeian F, Azadi S, Myers M, Pejcic B, Abbassi R, Razmjou A, Asadnia M, Chemosphere 2020, 259, 127492.

[54]. Zhu Y, Chen J, Yuan D, Yang Z, Shi X, Li H, Jin H, Ran L, TrAC Trends Anal. Chem. 2019, 119, 115627.

[55]. Zhu Y, Zheng J, Ye J, Cui Y, Koh K, Kovarik L, Camaioni DM, Fulton JL, Truhlar DG, Neurock M, Cramer CJ, Gutiérrez OY, Lercher JA, Nat. Commun. 2020, 11, 5849. [PubMed: 33208734]

[56]. Otake K, Cui Y, Buru CT, Li Z, Hupp JT, Farha OK, J. Am. Chem. Soc. 2018, 140, 8652–8656. [PubMed: 29950097]

[57]. Zhang J, Peh SB, Wang J, Du Y, Xi S, Dong J, Karmakar A, Ying Y, Wang Y, Zhao D, Chem. Commun. 2019, 55, 4727–4730.

[58]. Jiang J, Gándara F, Zhang Y-B, Na K, Yaghi OM, Klemperer WG, J. Am. Chem. Soc. 2014, 136, 12844–12847. [PubMed: 25157587]

[59]. Larsson M, Lindén JB, Kaur S, Cerf BL, Kempson I, Powder Diffr. 2017, 32, S28–S32.

[60]. Zhang R, Sun P, Boyer TH, Zhao L, Huang C-H, Environ. Sci. Technol. 2015, 49, 3056–3066. [PubMed: 25625668]

[61]. ISO 30500:2018. Non-sewered sanitation systems — Prefabricated integrated treatment units — General safety and performance requirements for design and testing.

[62]. Siegrist H, Laureni M, Udert KM, Source Sep. Decentralization Wastewater Manag. 2013, 337–350.

[63]. Zheng Z, Nguyen HL, Hanikel N, Li KK-Y, Zhou Z, Ma T, Yaghi OM, Nat. Protoc. 2023, 18, 136–156. [PubMed: 36289405]

[64]. Cline RE, Fink RM, Anal. Chem. 1956, 28, 47–52.

[65]. Jiang J, Gándara F, Zhang Y-B, Na K, Yaghi OM, Klemperer WG, J. Am. Chem. Soc. 2014, 136, 12844–12847. [PubMed: 25157587]

[66]. Thompson AP, Aktulga HM, Berger R, Bolintineanu DS, Brown WM, Crozier PS, in ‘t Veld PJ, Kohlmeyer A, Moore SG, Nguyen TD, Shan R, Stevens MJ, Tranchida J, Trott C, Plimpton SJ, Comput. Phys. Commun. 2022, 271, 108171.

[67]. Rappe AK, Casewit CJ, Colwell KS, Goddard WA, Skiff WM, J. Am. Chem. Soc. 1992, 114, 10024–10035.

[68]. Webb SM, Phys. Scr. 2005, 2005, 1011.

[69]. Ankudinov AL, Ravel B, Rehr JJ, Conradson SD, Phys. Rev. B 1998, 58, 7565–7576.

[70]. Cheah W-K, Sim Y-L, Yeoh F-Y, Mater. Chem. Phys. 2016, 175, 151–157.

[71]. Kameda T, Ito S, Yoshioka T, J. Dispers. Sci. Technol. 2017, 38, 1063–1066.

[72]. Pillai MG, Simha P, Gugalia A, J. Environ. Chem. Eng. 2014, 2, 46–55.

[73]. Severino MI, Gkaniatsou E, Nouar F, Pinto ML, Serre C, Faraday Discuss. 2021, 231, 326–341. [PubMed: 34254064]

[74]. Luther AK, Desloover J, Fennell DE, Rabaey K, Water Res. 2015, 87, 367–377. [PubMed: 26453942]

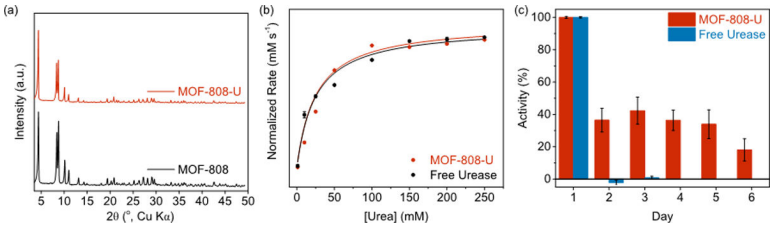

Figure 1.

(a) PXRD patterns of MOF-808-U and pristine MOF-808. The almost identical PXRD patterns indicate that the crystallinity of MOF structure was well-maintained during the incorporation of urease. (b) Michaelis–Menten kinetic measurement of MOF-808-U and free urease. MOF-808-U exhibited near-identical enzymatic activity to that of free urease. (c) Stability tests of MOF-808-U and free urease, where MOF-808-U demonstrated substantial stability (up to 6 days) compared to free urease.

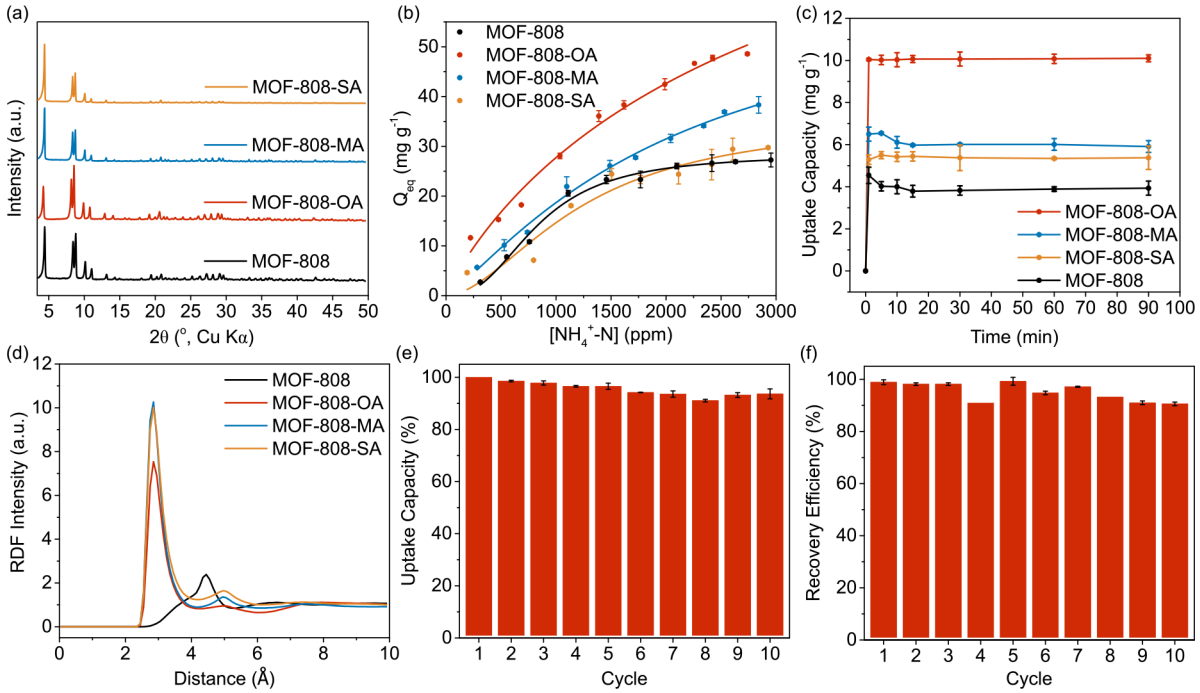

Figure 2.

(a) PXRD patterns, (b) ammonium uptake isotherms, and (c) uptake kinetics curves of MOF-808, MOF-808-OA, MOF-808-MA, and MOF-808-SA. While all four MOF materials shared an identical framework structure, modification of the interior pore environment has a direct and significant impact on their ammonium capture performances. (d) RDF analysis for nitrogen-oxygen distances in functionalized MOF-808 adsorbents and nitrogen-hydrogen distance in pristine MOF-808. (e) Ammonium uptake capacity and (f) recovery efficiency of MOF-808-OA with 10 cycles of regeneration, where sodium nitrate solution was used as the regenerant.

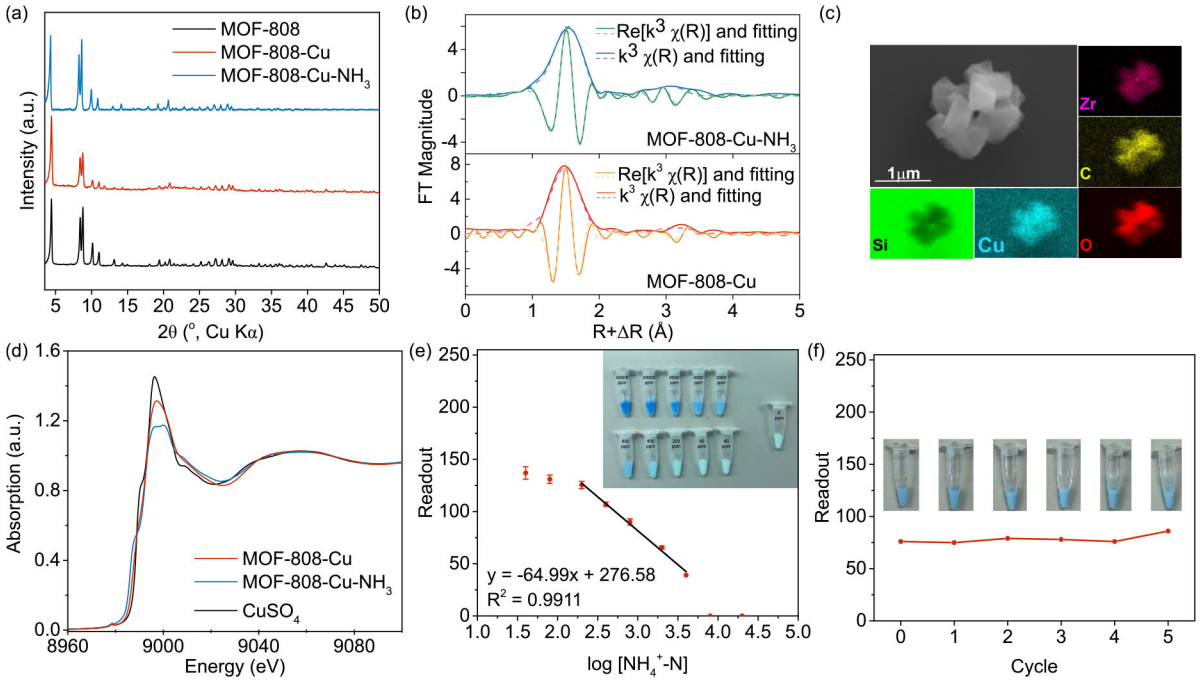

Figure 3.

(a) PXRD patterns of pristine MOF-808, MOF-808-Cu, and MOF-808-Cu exposed with [NH_3-N] of 2000 ppm (sample named as MOF-808-Cu-NH_3). (b) Fourier-transform magnitude and real phase of Cu K-edge k^3-weighted EXAFS with fitting lines for both MOF-808-Cu and MOF-808-Cu-NH_3. (c) SEM-EDS images of MOF-808-Cu showing Cu atoms are distributed homogeneously onto the MOF backbone. (d) Cu K-edge X-ray absorption near edge structure (XANES) spectra of MOF-808-Cu, MOF-808-Cu-NH_3, and $CuSO_4$. While MOF-808-Cu and $CuSO_4$ share similar spectra figure, MOF-808-Cu-NH_3 rendered a doublet absorbance around 9000 eV and a redshift of absorbance shoulder peak at 8990 eV, which is typically found in Cu-NH_3 coordination. (e) Linear relationship between the readout of the R channel and ammonia concentrations. Inset: an image of MOF-808-Cu suspended in a series of solutions with different [NH_3-N] levels. Concentrations from top left to bottom right are: 40000, 20000, 8000, 4000, 2000, 800, 400, 200, 80, and 40 ppm. The vial on the far right was MOF-808-Cu suspended in water only. (f) Readout of the R channel of MOF-808-Cu after 5 cycles of regeneration. Inset: an image of regenerated MOF-808-Cu suspended in a solution of 2000 ppm [NH_3-N].

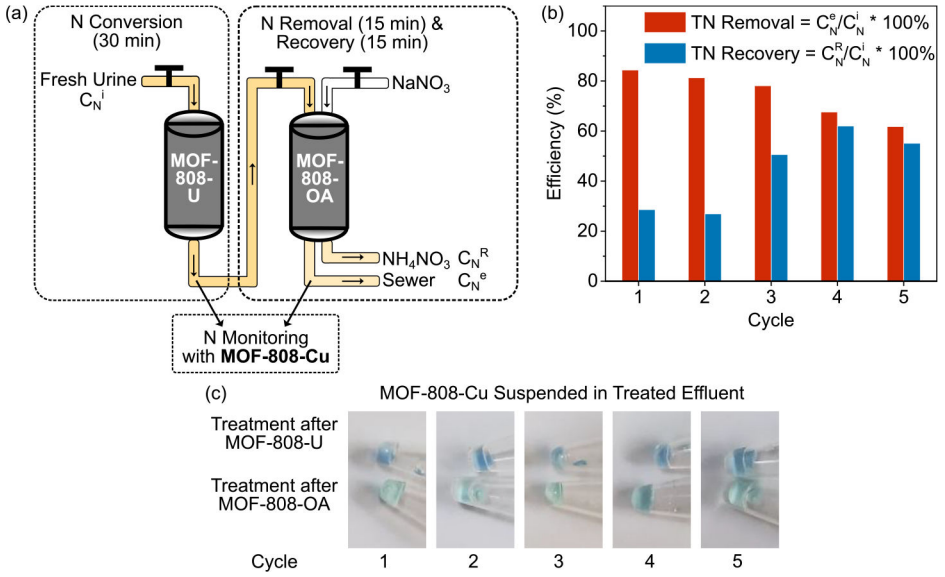

Figure 4.

(a) Schematic diagram of fresh urine nitrogen recovery integrating three functionalized MOF materials designed in this work. (b) Total nitrogen removal and recovery efficiency of five cycles of treatment. (c) MOF-808-Cu suspended in effluents after MOF-808-U (top) and MOF-808-OA (bottom) treatment in each of the five cycles, demonstrating the successful operation of each treatment step (urea conversion, ammonium capture, and regeneration of the ammonium adsorbent).

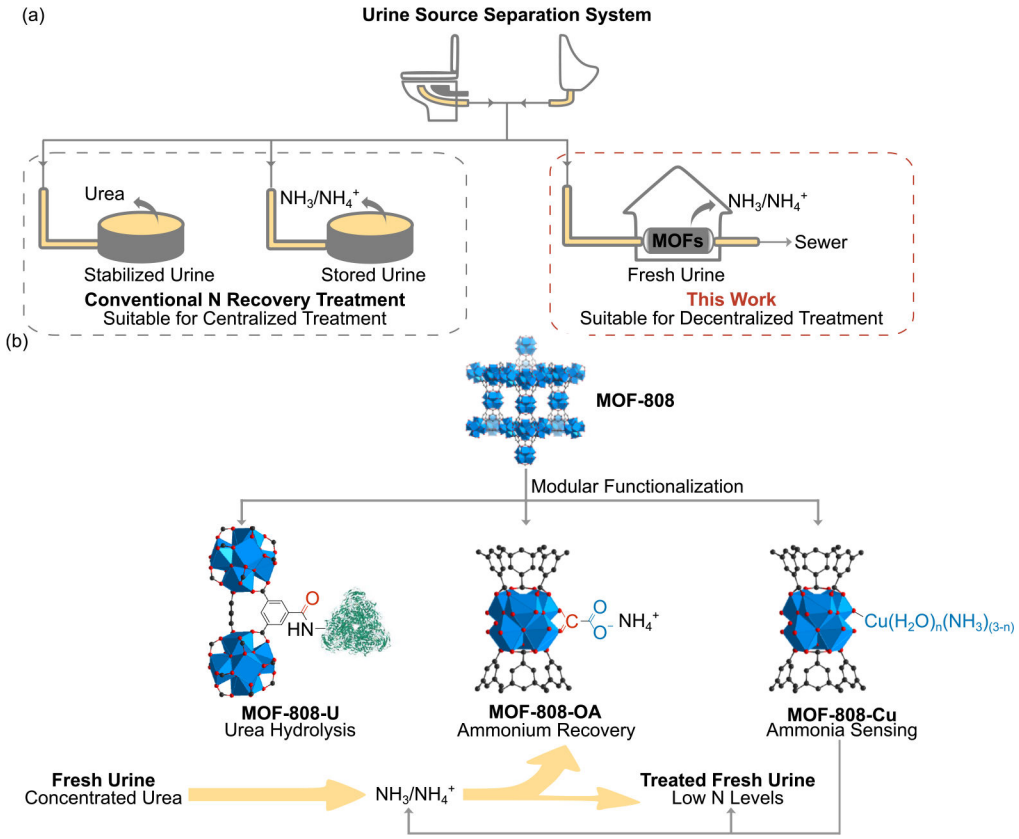

Scheme 1.

(a) Conventional and the newly developed nitrogen recovery treatment processes for urine source separation systems. (b) Schematic representation of how modular functionalized MOFs are designed and employed for nitrogen management in fresh urine.

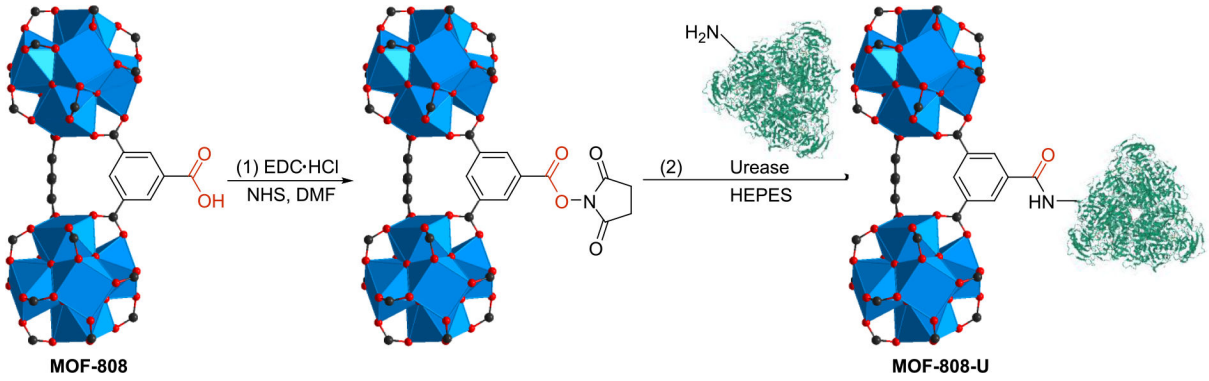

Scheme 2.

Synthesis scheme for MOF-808-U. The urease structure is obtained from pdb 4H9M.

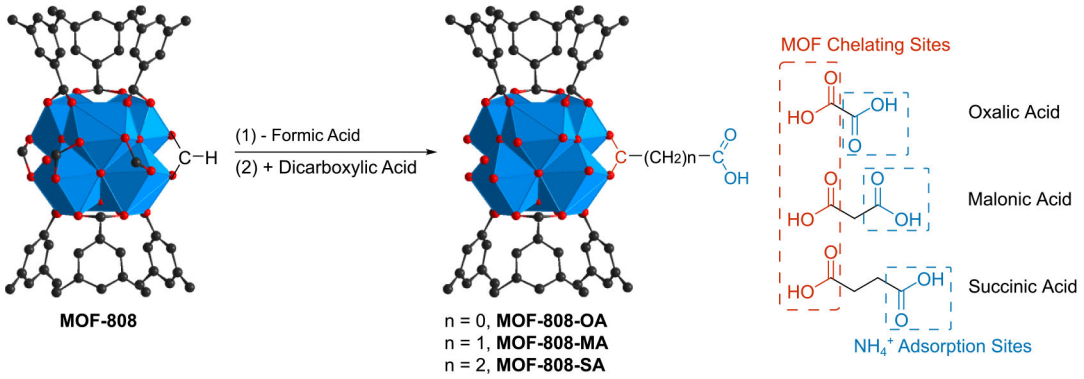

Scheme 3.

Synthesis scheme of MOF-808-based ammonium adsorbents, namely MOF-808-OA, MOF-808-MA, and MOF-808-SA.

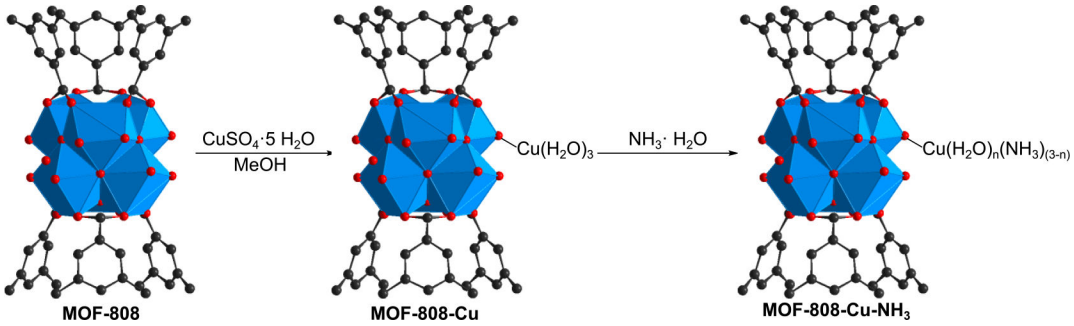

Scheme 4.

Schematic representation of Cu(II) incorporation onto MOF-808 and ammonia sensing process with MOF-808-Cu.